Formation of pericentromeric heterochromatin via ZNF518 that links satellite DNA to heterochromatin

Shinya Ohta[1,2]*, Jun-Ichirou Ohzeki[3], Nobuko Sato[2], Ken-Ichi Noma[1,4], and Hiroshi Masumoto[3]*

[1]Institute for Genetic Medicine, Hokkaido University, Kita-15, Nishi-7, Kita-Ku, Sapporo, 060-0815, Japan

[2]Department of Biochemistry, Medical School, Kochi University, Kohasu, Oko-cho, Nankoku, Kochi 783-8505, Japan

[3]Laboratory of Chromosome Engineering, Department of Frontier Research and Development, Kazusa DNA Research Institute, 2-6-7 Kazusa-Kamatari, Kisarazu 292-0818, Japan

[4]Institute of Molecular Biology, University of Oregon, 1370 Franklin Blvd., Eugene, OR 97403

***Corresponding authors:**

shinya.ohta@igm.hokudai.ac.jp

masumoto@kazusa.or.jp

Abstract

Aneuploidy is caused by chromosomal missegregation and frequently observed in cancers and hematological diseases. It is therefore important to understand the molecular mechanisms underlying chromosomal segregation. The intricate structure formed at the centromere or kinetochore plays an integral role in the segregation of chromosomes. For instance, heterochromatin present at pericentromeric alpha-satellites is essential for proper chromosomal segregation, although it is unclear how heterochromatin is targeted to pericentromeres. Here, we demonstrate a novel mechanism by which two homologous zinc-finger proteins (ZNF518A and ZNF518B) play central roles in heterochromatin formation at pericentromeres. We investigate this mechanism by determining the cellular localization of ZNF518, centromeric proteins such as CENP-A and CENP-B, and heterochromatin factors including HP1 and histone H3K9 trimethylation. The results indicate that the multiple segments within the ZNF518 contributes to their interactions with CENP-B, HP1, and G9a histone H3K9 methyltransferase. This study identifies a novel mechanism underlying pericentromeric heterochromatin formation, which is mediated by the central component, ZNF518.

KEYWORDS

centromere, pericentromeres, heterochromatin, ZNF518, CENP-B

Introduction

Defects in centromere or kinetochore functions are directly related to chromosomal abnormalities, and the anomalous segregation of chromosomes can lead to cancer or hematological diseases (Molina *et al*, 2020; Barra & Fachinetti, 2018). Chromosomal abnormalities can occur during mitosis, where replicated chromosomes are normally distributed equally between two daughter cells. During mitosis, compacted chromosomes are segregated when the spindle attaches to and pulls the kinetochore, a proteinaceous structure on the chromosome. The region of the chromosome that forms the kinetochore is the centromere. Centromere protein A (CENP-A), a centromere specific histone H3 variant, is essential for kinetochore formation on centromeres and directs the assembly of a complex containing at least 15 other proteins, including centromere protein C (CENP-C) (Cheeseman & Desai, 2008). The centromeric factors CENP-A, centromere protein B (CENP-B), and CENP-C are evolutionarily conserved from fission yeast to vertebrates and are known to localize at different parts of the centromere (McKinley & Cheeseman, 2016; Amor *et al*, 2004).

At the human centromere, CENP-A assembles onto portions of a large repetitive DNA locus containing a 171 bp repeat element also known as α-satellite DNA (alphoid DNA) (Waye & Willard, 1987). Some subclasses of alpha-satellite DNA contain a 17-nucleotide CENP-B box sequence that is bound by CENP-B (Masumoto *et al*, 2004; Earnshaw *et al*, 1987; Schueler & Sullivan, 2006). CENP-B and CENP-B boxes are required for human artificial chromosome formation and de novo centromeric CENP-A chromatin assembly when introducing alphoid DNA into cells

(Ohzeki *et al*, 2002; Okamoto *et al*, 2007; Okada *et al*, 2007). Furthermore, CENP-B is required for the assembly of CENP-A and CENP-C into centromeres, and consequently for functional centromere formation (Black & Cleveland, 2011; Cleveland *et al*, 2003). Most of the flanking satellite DNA regions (pericentromeres) are occupied by heterochromatin (Sullivan & Karpen, 2004). CENP-B also induces heterochromatin formation on pericentromeric alphoid DNA integrated into chromosomal arms (Okada *et al*, 2007). Interestingly, CENP-B recruits many factors in a mutually exclusive manner, including the open chromatin modifier ASH1L (H3K9 methylase) and heterochromatin factor HP1 (Otake *et al*, 2020). Heterochromatin is reported to have important roles in chromosome stability and maintenance of sister chromatid cohesion during chromosome segregation (Peters et al., 2001; Grewal and Jia,2007). Thus, both centromere chromatin and heterochromatin are important for accurate chromosome segregation processes.

Pericentromeric heterochromatin insulates centromeres from the rest of the genome and is required for the proper segregation of mitotic chromosomes(Molina *et al*, 2016; Grewal & Jia, 2007). Additionally, heterochromatin is known to have a more condensed structure than euchromatin and carries specific post-translational histone modifications. Nucleosomal surfaces with charge differences also contribute to the condensed structure of heterochromatin (Du & Patel, 2014; Hyun *et al*, 2017; Martin & Zhang, 2005). Furthermore, the trimethylation of histone H3 at lysine 9 (H3K9me3) is recognized and bound by the chromodomain of the heterochromatin protein HP1 (Canzio *et al*, 2011). HP1, in turn, recruits the suppressor of variegation 3-9 homolog

(SUV39H), which is an H3K9 methyltransferase (Peters *et al*, 2001; Rea *et al*, 2000). The HP1-mediated loading of SUV39H to chromatin is required for the maintenance of heterochromatin at pericentromeres (Aagaard *et al*, 1999; Muramatsu *et al*, 2016). Since SUV39H localizes to pericentromeres in addition to other constitutive heterochromatin regions, heterochromatin formation at pericentromeres involves SUV39H. The mechanisms by which heterochromatin factors are initially targeted to pericentromeres, however, remain elusive (Shirai *et al*, 2017).

Enzymes other than SUV39H have also been recognized as H3K9 methyltransferases. SET domain bifurcated 1 (SETDB1), for example, catalyzes H3K9me3 formation, while euchromatic histone lysine methyltransferase 1 and 2 (GLP and G9a) are responsible for H3K9me1 and H3K9me2, respectively. G9a can also methylate Lys9 and Lys27 of histone H3 (Tachibana *et al*, 2001). These H3K9 methyltransferases, including SUV39H, are selectively loaded onto distinct genomic regions through protein interactions with other factors (Fritsch *et al*, 2010). G9a and GLP bind to the widely interspaced zinc-finger (WIZ) protein (Ueda *et al*, 2006; Maier *et al*, 2015; Tachibana *et al*, 2001). It has been observed that H3K9 methylation at chromosomal arm regions is mostly lost in G9a-deficient cells, while H3K9 methylation at pericentromeres is largely lost in SUV39H-deficient cells (Tachibana *et al*, 2001). Moreover, the interaction between G9a and zinc-finger protein 518B (ZNF518B) was recently identified via a proteomics analysis (Maier *et al*, 2015). Our previous proteomics analysis revealed a possible role for ZNF518B as a functional protein on mitotic chromosomes (Ohta *et al*, 2010a, 2016). The present study demonstrates that

G9a, which acts as a H3K9 methyltransferase for chromosomal arm regions, is also involved in heterochromatin formation at pericentromeres via its interaction with ZNF518B (which is targeted to pericentromeres by CENP-B).

Results

Human ZNF518A/B are localized to centromeres via CENP-B

We first examined the localization of green fluorescent protein (GFP)-tagged ZNF518B and the centromeric factors CENP-A, CENP-B, and CENP-C in human U2OS cells. The advantage of overexpression of GFP fusion proteins is that it allows for enhanced visualization of even low-expression proteins, and with this technique we were able to successfully demonstrate the visualization of the localization of ZNF518. Surprisingly, GFP-ZNF518B co-localized proximally to the centromeric factors (Fig. 1A–F). In addition, ZNF518B localized to the centromeres during mitosis (Fig. S1A). The GFP-ZNF518B foci were slightly shifted from the CENP-A and CENP-C foci but coincided with the CENP-B foci, suggesting that ZNF518B localizes to centromeres and pericentromeres bound by CENP-B (Fig. 1A–F).

To investigate the localization dependency between ZNF518B and CENP-B, we examined the localization of GFP-ZNF518B in CENP-B knockout (KO) HeLa cells (Otake *et al*, 2020). GFP-ZNF518B did not localize at the centromeres in the CENP-B KO cells (Fig. 1G, H); however, its localization at the centromeres was restored when exogeneous CENP-B was expressed in the CENP-B KO cells (Fig. 1I). These results indicate that the centromeric localization of ZNF518B depends on CENP-B.

ZNF518A is a paralogue of ZNF518B that is present in humans (Fig. S1B). To determine the localization of ZNF518A, GFP-ZNF518B and Halo-ZNF518A were transiently co-expressed in U2OS cells (Fig. 1J). The GFP-ZNF518B and Halo-

ZNF518A foci co-localized at the centromeres. Again, the co-localized signals were slightly shifted from the CENP-A foci, suggesting that both ZNF518A/B localize at centromeres (Fig. 1J). Moreover, GFP-ZNF518A did not localize at the centromeres in the CENP-B KO cells, and centromeric localization was restored when exogenous CENP-B was expressed (Fig. S1C). These indicated that the centromeric localization of ZNF518A depends on CENP-B. Taken together, our results suggest that either the two ZNF518 proteins, ZNF518A and ZNF518B, localize to centromeres and centromere via a common molecular mechanism involving CENP-B, or that ZNF518A and ZNF518B interact and are recruited to centromeres and pericentromere by CENP-B (Fig. S1D).

The C-terminal segment of ZNF518A/B is required for centromeric localization

To gain insights into the molecular mechanisms underlying the recruitment of ZNF518 to centromeres, we sought to identify the segments within ZNF518B that are required for centromeric localization. We examined the centromeric localization of 15 derivatives of ZNF518B expressed as GFP fusion proteins (Fig. 2). ZNF518B comprises 1,074 amino acids (aa). The ZNF518B derivatives that contained the regions from the N-terminus to 628 aa (ZNF518B$^{1-398}$, ZNF518B$^{344-628}$, and ZNF518B$^{1-628}$) did not show centromeric localization (Fig. 2, S2A). Thus, the N-terminus of ZNF518B does not form sufficient interactions to localize the protein to centromeres.

Upon assessing the centromeric localization of the four ZNF518B derivatives (ZNF518B$^{344-1074}$, ZNF518B$^{344-987}$, ZNF518B$^{344-877}$, and ZNF518B$^{344-769}$) with

incrementing C-terminal truncations, we found that three derivatives (ZNF518B$^{344-1074}$, ZNF518B$^{344-987}$, and ZNF518B$^{344-877}$) showed centromeric localization in 70.7%, 58.9%, and 57.1% of the transfected cells, respectively (Fig. 2). In sharp contrast, ZNF518B$^{344-769}$ did not show centromeric localization (Fig. 2). Similarly, among the three derivatives ZNF518B$^{555-1074}$, ZNF518B$^{555-877}$, and ZNF518B$^{555-769}$, only ZNF518B$^{555-769}$, which has the same C-terminal truncation as ZNF518B$^{344-769}$, did not show centromeric localization (Fig. 2, S2A). These results suggest that residues 770–877 of ZNF518B are deeply involved in its centromeric localization. However, only 2.2% of the transfected cells showed the centromeric localization of ZNF518B$^{770-877}$ (Fig. 2). Thus, residues 770–877 are important, but insufficient, for centromeric localization.

As there was a large difference in the percentage of cells localized to the centromere with ZNF518B$^{555-1074}$, ZNF518B$^{555-877}$, and ZNF518B$^{555-769}$ (64.5%, 31.8%, and 0% of the cells, respectively), we examined the centromeric localization of ZNF518B derivatives that carried residues 770–1074 (Fig. 2, S2A). The three ZNF518B derivatives ZNF518B$^{878-1074}$, ZNF518B$^{878-987}$, and ZNF518B$^{770-987}$ showed centromeric localization to varying degrees (53.6%, 56.7%, and 89.3%, respectively; Fig. 2, S2A). ZNF518B$^{770-987}$ showed the highest frequency of centromeric localization among all the ZNF518B derivatives. These results collectively suggest that residues 770–987 are involved in the centromeric localization of ZNF518B.

We next examined the centromeric localization of several ZNF518A derivatives (Fig. S2B). The wild-type (WT) ZNF518A ($ZNF518A^{WT}$) and two derivatives ($ZNF518A^{971-1483}$ and $ZNF518A^{1317-1483}$) containing the C-terminal 1317–1483-aa segment showed high frequencies of centromeric localization, suggesting that the C-terminal portion of ZNF518A harbors crucial segment(s) for centromeric localization (Fig. S2B). Notably, the C-terminal segments of ZNF518A and ZNF518B required for centromeric localization carried PxV(I)xL HP1-interaction motifs, which are widely conserved among higher vertebrates, including fish. This implied their evolutionarily conserved role potentially through their localization at centromeres (Fig. S3).

The C-terminal PxIxL motif is required for the centromeric localization of ZNF518B

To elucidate the functional significance of the PxV(I)xL motifs in ZNF518B, we constructed the GFP-$ZNF518B^{KSS/C}$ derivative and substituted the conserved hydrophobic residues PxIxL in the C-terminal segment with the hydrophilic residues KxSxS (Fig. 2). $ZNF518B^{KSS/C}$ exhibited impaired centromeric localization (14.3%) compared to $ZNF518^{WT}$ (77.5%; Fig. 2). In contrast, the centromeric localization of $ZNF518B^{KSS/N}$, which carries a KxSxS substitution at the PxVxL motif in the N-terminal segment, was comparable to that of $ZNF518^{WT}$ (Fig. 2). $ZNF518B^{KSS/NC}$, which carries the KxSxS substitutions for the PxV(I)xL motifs in both the N- and C-terminal segments, showed a similar frequency of centromeric localization (21.4%) as the $ZNF518B^{KSS/C}$ derivative (Fig. 2). The PxIxL motif present in the C-terminal, but not in the N-terminal, is therefore involved in the centromeric localization of ZNF518B. $ZNF518A^{KSS}$, which

carries a KxSxS substitution at the PxVxL motif in the C-terminal, also showed impaired centromeric localization (Fig. S2B). These results demonstrate that the conserved PxV(I)xL motif in the C-terminal region of ZNF518 is important for centromeric localization.

Although the C-terminal PxIxL motif is important for centromeric localization, both ZNF518B$^{KSS/C}$ and ZNF518B$^{KSS/NC}$ could localize at the centromeres in 14.3% and 21.4% of the cells, respectively, implying the involvement of other interactions in centromeric localization (Fig. 2, S2B). To test this notion, we used the ZNF518B$^{770-987}$ derivative that localized to centromeres with the highest frequency and substituted the PxVxL motif in the C-terminal segment with KxSxS. This yielded the new derivative, ZNF518B$^{770-987\ KSS/C}$. Notably, although reduced, ZNF518B$^{770-987\ KSS/C}$ still showed centromeric localization in 60.6% of the transfected cells (Fig. 2, S2B). These results reveal that both the PxIxL motif and C-terminal segment (770–987 aa) participate in the centromeric localization of ZNF518B.

ZNF518B interacts with HP1α and HP1β

The localization of full-length ZNF518B^{WT} to centromeres and also pericentromeres requires CENP-B. The ZNF518B$^{770-987}$ derivative, with the C-terminal segment (770–987 aa) that includes the PxIxL motif, also localizes to centromeres (Fig. 2). In CENP-B KO cells, ZNF518B$^{770-987}$ showed focal localization that was not observed for ZNF518B^{WT} (Fig. S4A). However, the ZNF518B$^{770-987}$ foci were distinct from centromeres. These foci were found to co-localize with the heterochromatin foci in the

CENP-B KO cells (Fig. S4B). Thus, ZNF518B$^{770-987}$ can be recruited to non-pericentromeric heterochromatin domains through its interaction with heterochromatic factors in the absence of CENP-B (Fig. S4C).

Given its similarity to the canonical HP1-interacting motif PxVxL, we hypothesized that the PxIxL motif in the C-terminal segment of ZNF518B interacts with HP1, thereby resulting in the accumulation of ZNF518B at heterochromatin regions in CENP-B KO cells. There are three isozymes of human HP1: HP1α, HP1β, and HP1γ (Canzio et al., 2014). We attempted to characterize the interaction between ZNF518B and the HP1 isoforms using the fluorescence microscopy-based interaction-trap (FMIT) assay (Ohzeki *et al*, 2016). The FMIT assay may be used to examine protein interactions on chromatin *in vivo*. Given the overabundance of target proteins compared to their endogenous counterparts, this technique allows for the detection of direct and indirect protein–protein interactions using fluorescence microscopy (Ohzeki *et al*, 2012; Otake *et al*, 2020; Molina *et al*, 2016; Bergmann *et al*, 2011; Martins *et al*, 2016; Ohzeki *et al*, 2016; Shono *et al*, 2015).

The FMIT assay was performed to test the interaction between ZNF518B and HP1 isoforms in HeLa-Int-03 cells. In the HeLa-Int-03 cells, approximately 15,000 repeats of the synthetic alphoid DNA dimer unit (derived from the human chromosome 21 centromere) containing the tetO sequence (alphoid^{tetO}) were ectopically integrated into a chromosome arm region, and CENP-B was knocked out (Fig. 3A) (Otake *et al*, 2020). TetR-EYFP-ZNF518B localized to the alphoid^{tetO} repeats but did not exhibit

centromeric localization due to the absence of CENP-B. We next examined whether Halo-HP1 co-expressed with TetR-EYFP-ZNF518B would be recruited to the alphoid^{tetO} array (Fig. 3B). Halo-HP1α, -HP1β, and -HP1γ were recruited to the alphoid^{tetO} in 48%, 58%, and 14% of the cells, respectively (Fig. 3C). In the negative controls where TetR-EYFP not fused to ZNF518B was expressed, Halo-fused HP1α, HP1β, and HP1γ were barely recruited to the alphoid^{tetO} (Fig. 3C). These results suggest that ZNF518B interacts with HP1.

The PxIxL motif in the C-terminal segment of ZNF518B interacts with HP1 isoforms

We next investigated the segments within ZNF518B that are required to interact with the HP1 isoforms by subjecting the ZMF518B derivatives described in Figure 1 to the FMIT assay (Fig. 3C). Upon co-expressing Halo-HP1 and TetR-EYFP-fused ZNF518B derivatives (ZNF518B$^{1-398}$, ZNF518B$^{1-628}$, ZNF518B$^{344-628}$, ZNF518B$^{344-877}$, ZNF518B$^{555-877}$, and ZNF518B$^{770-877}$), Halo-HP1 was either scarcely or not recruited to the alphoid^{tetO}. Since these derivatives are devoid of the PxIxL motif, this result implies the importance of the PxIxL motif in the interactions between ZNF519B and the HP1 isoforms (Fig. 3C).

To further examine the significance of the PxV(I)xL motifs in the ZNF518B-HP1 interactions, TetR-EYFP-fused ZNF518B derivatives (ZNF518B$^{KSS/N}$, ZNF518B$^{KSS/C}$, ZNF518B$^{KSS/NC}$, and ZNF518B$^{770-987\ KSS/C}$) were used for the FMIT assay. These derivatives carry the substitutions of the PxV(I)xL motifs with KxSxS, as depicted in

Figure 1. Halo-HP1 was scarcely recruited to the alphoid^{tetO} by the ZNF518B derivatives, apart from ZNF518B$^{KSS/N}$. The PxIxL motif in the C-terminal segment, but not the PxVxL motif in the N-terminal segment, therefore participates in the interactions with HP1 (Fig. 3C).

Next, the TetR-EYFP-fused ZNF518B derivatives ZNF518B$^{344-1074}$, ZNF518B$^{344-987}$, ZNF518B$^{555-1074}$, ZNF518B$^{878-1074}$, ZNF518B$^{878-987}$, and ZNF518B$^{770-987}$ were used for the FMIT assay. All these derivatives carry the PxIxL motif in the C-terminal segment of ZNF518B. We observed that Halo-HP1 was recruited to the alphoid^{tetO} in more than 75% of the cells (Fig. 3C). Remarkably, these N-terminal-deleted derivatives were able to recruit the three distinct HP1 proteins with similar frequencies. Furthermore, ZNF518B$^{344-1074}$ was more efficient at recruiting HP1 than ZNF518B^{WT}. The N-terminal segment (1–398) is therefore inhibitory for the ZNF518B interactions with HP1 isoforms (Fig. 3C).

The PxIxL motif of ZNF518B interacts with the chromo-shadow domain of HP1

HP1 consists of a central linker flanked by chromo and chromo-shadow domains, the latter of which interacts with the PxVxL motif in CAF1/p150 (Thiru *et al*, 2004). Since the PxIxL motif in ZNF518B plays a vital role in the interactions with HP1 isoforms, we predicted that ZNF518B may interact with the chromo-shadow domain rather than the chromo domain of HP1 isoforms. Using the FMIT assay, we examined the interaction between ZNF518B and the chromo domain (HP1β^{1-92}) or chromo-shadow domain (HP1β^{93-185}) of HP1β. As expected, the chromo-shadow domain, but

not the chromo domain, was recruited to the alphoid^{tetO} by ZNF518B derivatives carrying the PxIxL motif in the C-terminal segment. This confirmed the interaction between the PxIxL motif of ZNF518B and chromo-shadow domain of HP1β (Fig. 3C).

ZNF518B$^{344-769}$ and ZNF518B$^{555-769}$ weakly bound HP1β despite the absence of a PxIxL motif. Indeed, the PxIxL motif of ZNF518B had similar binding affinities for all three HP1 isoforms. However, residues 971–1321 of ZNF518A, which correspond to residues 555–769 of ZNF518B, did not show such specificity for the HP1 isoforms (Fig. S5A). The 555–769-aa segment in ZNF518B is therefore a subsidiary segment for the HP1 interactions that determine its specificity for HP1β.

ZNF518B maintains HP1 on chromatin

We next examined whether HP1β loaded to the alphoid^{tetO} by TetR-EYFP-ZNF518B is maintained at the alphoid^{tetO} at the repeat locus when ZNF518B is released from the alphoid^{tetO} following the addition of doxycycline (Dox) (Fig. 3D). TetR-EYFP-ZNF518 was rapidly released from the alphoid^{tetO} after introducing Dox. EYFP foci disappeared in 96% of the cells 120 min after Dox introduction (Fig. S5B). We further quantified the presence of Halo-HP1β foci at the alphoid^{tetO} 150 min after the introduction of Dox (Fig. 3E). The Halo-HP1β foci disappeared from the alphoid^{tetO} in all experiments employing ZNF518B^{WT}, ZNF518B$^{878-987}$, and ZNF518B$^{770-987}$ (Fig. 3E). ZNF518B is therefore required to maintain HP1β at the alphoid^{tetO}.

ZNF518B interacts directly with HP1 isoforms *in vitro*

The above FMIT results strongly suggest that ZNF518B interacts with HP1 isoforms. To further examine their direct interactions, we expressed the ZNF518B$^{770-987}$ derivative containing the PxIxL motif at the C-terminal segment in *Escherichia coli* cells. ZNF518B$^{770-987}$ proteins fused to histidine affinity tag (HAT) and maltose-binding protein (MBP) tags were purified using Ni-NTA resin. HP1 isoforms fused to both His_6 and glutathione S-transferase (GST) tags were purified from *E. coli* cells using Ni-NTA resin. The two purified proteins were mixed, and the MBP-fused ZNF518B$^{770-987}$ proteins were pulled-down (PD) using magnetic amylose beads. We observed that the HP1 isoforms were co-purified with ZNF518B$^{770-987}$. The GST-HP1 isoforms were more abundant in the PD samples with MBP-ZNF518B$^{770-987}$ than in those with MBP alone (Fig. 3F). These results suggest that the PxIxL motif at the C-terminal segment of ZNF518B directly interacts with HP1α, HP1β, and HP1γ (Fig. 3G).

ZNF518B localization cannot be maintained at centromeres without CENP-B

The previous results (Fig. 1) showed that CENP-B is required for ZNF518B localization at centromeres. Based on this observation, we next investigated whether CENP-B is required to maintain ZNF518B at centromeres. We created a CENP-B conditional KO system using human U2OS cells (Fig. S6A). The gene expressing *Oryza sativa* TIR1 was inserted into an adeno-associated virus genomic integration site. In these cells, the endogenous CENP-B fused with a mini auxin-inducible degron (mAID) tag could be rapidly targeted for degradation via the ubiquitin-proteasome pathway following indole-3-acetic acid (IAA) treatment (Natsume *et al*, 2016).

The subsequent analysis was conducted under three conditions (Fig. 4A): CENP-B:mAID remained available at all times (CENP-B^{ON}); CENP-B:mAID was removed 24 h prior to ZNF518B transfection (CENP-B^{OFF}); and CENP-B:mAID was removed 4 h before fixation (CENP-B$^{4h\text{-}OFF}$). We examined the localization of GFP-ZNF518B under these three conditions. As expected, GFP-ZNF518B localized at the centromeres in CENP-B^{ON} cells (Fig. 4B–E). In CENP-B^{OFF} cells, the CENP-B signals at the centromeres were below the detection limit, and GFP-ZNF518B dissociated from the centromeres (Fig. 4B–E). In the CENP-B$^{4h\text{-}OFF}$ cells, GFP-ZNF518B also dissociated from the centromeres (Fig. 4B–E). These results demonstrate that the recruitment and maintenance of ZNF518B at centromeres requires CENP-B.

The interaction between ZNF518B and CENP-B

We examined the interaction between ZNF518B and CENP-B using the FMIT assay. For this purpose, we constructed Halo-CENP-B$^{133\text{-}599}$, which is devoid of the helix-turn-helix domain and thus cannot bind to alpha-satellites at centromeres (Otake *et al*, 2020). Halo-CENP-B$^{133\text{-}599}$ and TetR-EYFP-ZNF518B (WT and derivatives) were co-expressed in HeLa 03 Int cells (Fig. 4F). As expected, Halo-CENP-B$^{133\text{-}599}$ did not localize to centromeres. Therefore, CENP-B$^{133\text{-}599}$ foci reflect the recruitment of CENP-B to the alphoid^{tetO} by TetR-EYFP-ZNF518B.

We observed that CENP-B$^{133\text{-}599}$ was recruited to the alphoid^{tetO} in 26% of the cells expressing ZNF518B^{WT}, despite CENP-B$^{133\text{-}599}$ not being recruited to the loci in

cells expressing TetR-EYFP and lacking ZNF518B. This was consistent with the interaction between ZNF518B and CENP-B (Fig. 4G). In addition, CENP-B$^{133-599}$ was barely recruited at the alphoid^{tetO} by ZNF518B$^{1-398}$, ZNF518B$^{1-628}$, and ZNF518B$^{344-628}$, suggesting that the ZNF518B segment from 629 aa to the C-terminus is important for the interaction. Moreover, CENP-B$^{133-599}$ was recruited to the alphoid^{tetO} at high frequencies in cells expressing ZNF518B$^{344-1074}$, ZNF518B$^{344-987}$, ZNF518B$^{344-877}$, ZNF518B$^{555-1074}$, ZNF518B$^{555-877}$, ZNF518B$^{770-987}$, and ZNF518B$^{770-877}$, all of which contain residues 770–877 (Fig. 4G). Moreover, the recruitment frequencies of CENP-B$^{133-599}$ were reduced by 20% when cells either expressing ZNF518$^{344-877}$ or ZNF518$^{344-769}$ were compared, and by 39% when cells expressing ZNF518$^{555-877}$ or ZNF518$^{555-769}$ were compared. ZNF518B$^{878-1074}$ and ZNF518B$^{878-987}$, which do not carry residues 770–877 of ZNF518B, did not exhibit CENP-B$^{133-599}$ recruitment. These results support the importance of residues 770–877 of ZNF518B to its interaction with CENP-B (Fig. 4H).

We next examined the recruitment of CENP-B to the alphoid^{tetO} in cells expressing the ZNF518 derivatives ZNF518B$^{KSS/N}$, ZNF518B$^{KSS/C}$, ZNF518B$^{KSS/NC}$, and ZNF518B$^{770-987\ KSS/C}$ and carrying substitutions of the PxV(I)xL motifs with KxSxS (Fig. 4G). The substitutions of the PxV(I)xL motifs generally increased the recruitment of CENP-B to the *tetO* repeats. This implies an inhibitory role of the PxV(I)xL motifs in the interaction between ZNF518B and CENP-B. Although the association of ZNF518B with both HP1 and CENP-B is less effective in the full-length protein, the derivatives with the N-terminal region deleted showed considerably stronger interactions. We

speculate that this is because the interaction domain in some ZNF518 segments is exposed on the surface of the protein, allowing for easier interactions with the binding partner.

The C-terminal segment of ZNF518B interacts with G9a

Published proteomics data have revealed an interaction between ZNF518B and G9a (EHMT2) (Maier *et al*, 2015). We therefore attempted to identify the segments of ZNF518B that interact with G9a and vice versa. We used the FMIT assay with cells co-expressing EYFP-TetR-ZNF518 and Halo-G9a. The control experiment showed that G9a was recruited to *tetO* repeats in cells expressing ZNF518B^{WT} (Fig. S6C and 5A). G9a was recruited to the alphoid^{tetO} at high frequencies in cells expressing ZNF518B$^{KSS/C}$, ZNF518B$^{KSS/NC}$, ZNF518B$^{344-1074}$, ZNF518B$^{555-1074}$, and ZNF518B$^{878-1074}$ (Fig. 5A). In contrast, G9a was barely recruited to the alphoid^{tetO} by the other ZNF518B derivatives (Fig. 5A). Residues 988–1074 of ZNF518B are therefore crucial for its interaction with G9a.

We also performed FMIT experiments to examine the interaction between ZNF518A and G9a. We observed that G9a was recruited to the alphoid^{tetO} in cells expressing ZNF518A^{WT}, ZNF518A^{KSS}, ZNF518A$^{971-1483}$, ZNF518A$^{971-1483\ KSS}$, ZNF518A$^{1317-1487}$, and ZNF518A$^{1317-1483\ KSS}$ (Fig. 5B). However, G9a was less efficiently recruited to the alphoid^{tetO} in cells expressing ZNF518A$^{1-970}$ and ZNF518A$^{971-1321}$ compared to the other derivatives (Fig. 5B). These results suggest that residues 1317–1483 are important for the interaction between ZNF518A and G9a.

When combined with previous results, our data indicate that the C-terminal segments within ZNF518 are required for its interaction with G9a.

The segment present downstream of the TAD in G9a interacts with ZNF518A/B

Interactions between G9a and the C2H2-type zinc-finger motifs in ZNF644 and ZNF803, also known as Widely interspaced zinc finger (WIZ)-containing proteins, have previously been reported (Simon *et al*, 2015; Ueda *et al*, 2006). The zinc-finger motifs in WIZ-containing proteins also interact with the transcriptional regulatory CCAAT/enhancer-binding protein-β (C/EBPβ) transactivation domain (TAD) within the N-terminal segments of G9a and GLP (Bian *et al*, 2015). Since zinc-finger motifs are conserved in the C-terminal segments of ZNF518A/B that interact with G9a, we hypothesized that the C-terminal segments of ZNF518A/B may interact with the TAD of G9a.

To test this hypothesis, we performed FMIT experiments with several G9a derivatives (Fig. 5C). In contrast with the above prediction, we found that G9a$^{1\text{-}290}$ was not recruited to the alphoid^{tetO} by ZNF518A/B. Instead, G9a$^{291\text{-}1210}$, which lacks a TAD, was recruited to the alphoid^{tetO} by ZNF518A/B. Moreover, the two 291–545-aa segments containing the G9a derivatives, G9a$^{1\text{-}545}$ and G9a$^{291\text{-}545}$, were recruited to the alphoid^{tetO} by ZNF518A/B. These results indicate that residues 291–545 of G9a, but not the TAD, are sufficient for the interactions with ZNF518A/B.

The N-terminal residues 1–624 aa of ZNF518B did not interact with CENP-B, HP1, or G9a, nor did they exhibit centromeric localization. However, the N-terminal residues 1–970 aa of ZNF518A retained their centromeric localization with an observed interaction with HP1 and less effective interaction with CENP-B and G9a (Fig. S6B). ZNF518A and ZNF518B may therefore differ in terms of the functions of their N-terminal segments.

Finally, we assessed the possibility of the recruitment of G9a to centromeres by ZNF518. Plasmids expressing GFP-ZNF518B or ZNF518B derivatives and Halo-G9a were co-transfected into U2OS cells, and the localization of Halo-G9a was investigated (Fig. 5D). The localization of Halo-G9a at centromeres was observed only when Halo-G9a was expressed with WT or ZNF518B$^{344\text{-}1074}$ carrying the C-terminal segment, as revealed by the FMIT assay (Fig. 5D). However, the localization of Halo-G9a at centromeres was no longer observed when ZNF518B$^{344\text{-}987}$ lacking the C-terminal zinc-finger was expressed (Fig. 5D). Furthermore, no localization of Halo-G9a at centromeres was observed when GFP-ZNF518B and Halo-G9a were expressed in CENP-B KO cells (Fig. 5E). CENP-B therefore recruits ZNF518B to centromeres, and ZNF518B in turn recruits G9a H3K9 methyltransferase (Fig. 5F).

Discussion

In this study, we show that the 770–877 segment within ZNF518B interacts with CENP-B (Fig. 4G) and is recruited to centromeres and pericentromeres in a CENP-B-dependent manner (Fig. 1, 2, 4). Furthermore, the 555–765 segment and PxIxL motif within ZNF518B are required for its interaction with the chromo-shadow domain of HP1β (Fig. 3). The C-terminal segment carrying the ZF motif within ZNF518B interacts with the segment downstream of TAD within G9a, and CENP-B is required for the localization of G9a at centromeres (Fig. 5). Based on these observations, we propose the following mechanisms: 1) CENP-B binds to alpha-satellite DNA to initiate the establishment of heterochromatin; 2) CENP-B recruits ZNF518B to centromeres and pericentromeres; 3) H1Pβ in turn stabilizes ZNF518 only at pericentromeres; and 4) ZNF518B interacts with G9a to introduce H3K9me3 to pericentromeres.

The proposed mechanisms do not disagree with the previously proposed mechanism involving SUV39H1 histone H3K9 methyltransferase. It has been reported that HP1-dependent SUV39H1 recruitment and short RNA-mediated heterochromatinization are important for the maintenance of pericentromeric heterochromatin (Muramatsu et al., 2016; Shirai et al., 2017). Meanwhile, we propose that G9a recruited by CENP-B and ZNF518B is required for the establishment of pericentromeric heterochromatin, even though the interplay between the underlying mechanisms needs to be further elucidated. Although it has been unclear how heterochromatin is targeted to human pericentromeres, our study provides potential insights into the underlying mechanisms. We suggest that the CENP-

B/ZNF518B/HP1β/G9a axis can target heterochromatin factors to pericentromeres, where specificity is yielded by the binding of CENP-B to CENP-B box sequences in pericentromeric alphoid repeats.

In addition to ZNF518B, ZNF518A is recruited to pericentromeres in a CENP-B-dependent manner (Fig. S1) and interacts with HP1 and G9a (Fig. 5, S5). ZNF518A and ZNF518B are further evolutionarily conserved in all vertebrates higher than amphibians. Therefore, we speculate that pericentromeric heterochromatin formation by ZNF518 is conserved among many vertebrates.

Materials and Methods

DNA constructs

To clone the target genes, DNA fragments encoding human ZNF518A, ZNF518B, CENP-B$^{133-599}$, HP1α, HP1β, HP1γ, and G9a were amplified with the primers listed in Table S1 using PCR on the cDNA library, which was generated by the Kazusa ORFeome Project and Genome Network Project Clones by RIKEN BRC. The fragments were then inserted into the entry vector (pENTR™ 4 Dual Selection Vector; #A10465, Thermo Fisher Scientific) between the *Xmn*I [#R0194S, New England BioLabs (NEB)] and *EcoR*V (#R0195S, NEB) sites using the In-Fusion HD Cloning Kit (#Z9648N, Takara Bio). The entry plasmids pENTR4XE153, pENTR4XE127, pENTR4ΔCENPB, pENTR4HP1α, pENTR4HP1β, pENTR4HP1γ, and pENTR4G9a were then obtained, which comprised open reading frames encoding ZNF518A, ZNF518B, CENP-B$^{133-599}$, HP1α, HP1β, HP1γ, and G9a, respectively (Itoh *et al*, 2006; Nagase *et al*, 2008; Kimura *et al*, 2006; Otsuki *et al*, 2005; Ota *et al*, 2004).

To generate derivatives of the target genes, DNA fragments encoding ZNF518A derivatives (ZNF518A^{KSS}, ZNF518A$^{1-970}$, ZNF518A$^{971-1483}$, ZNF518A$^{971-1483KSS}$, ZNF518A$^{971-1321}$, ZNF518A$^{1317-1483}$, and ZNF518A$^{1317-1483KSS}$), ZNF518B derivatives (ZNF518B$^{KSS/N}$, ZNF518B$^{KSS/C}$, ZNF518B$^{KSS/NC}$, ZNF518B$^{1-398}$, ZNF518B$^{1-628}$, ZNF518B$^{344-628}$, ZNF518B$^{344-1074}$, ZNF518B$^{344-987}$, ZNF518B$^{344-877}$, ZNF518B$^{344-769}$, ZNF518B$^{555-985}$, ZNF518B$^{555-877}$, ZNF518B$^{555-769}$, ZNF518B$^{878-1074}$, ZNF518B$^{878-987}$, ZNF518B$^{770-987}$, ZNF518B$^{770-987KSS/C}$, and ZNF518B$^{770-877}$), HP1β derivatives (HP1β$^{N(1-92)}$ and HP1β$^{C(93-185)}$), and G9a derivatives (G9a$^{1-92}$ and G9a$^{93-185}$) were

amplified using PCR on pENTR4XN153, pENTR4XN127, pENTR4HP1β, and pENTR4G9a, respectively, with the primers listed in Table S1.

To overexpress the target proteins in human or *E. coli* cells, plasmids were generated by exploiting DNA recombination between the above-mentioned entry plasmids and pDEST131NGFP (to express EGFP fusion proteins (Ohta *et al*, 2015)), pDEST152JTY (to express EYFP-TetR fusion proteins), pDEST155Halo (to express Halo-tagged proteins), pDEST174HATMBP {to express HAT (KDHLIHNVHKEEHAHNK)-MBP fusion proteins (Chaga *et al*, 1999)}, or pDEST172HGST {to express His_6-GST fusion proteins using the Gateway LR Clonase II Enzyme mix (#11791020, Thermo Fisher Scientific)}.

To introduce CRISPR-mediated double-strand break sites, 54-bp DNA fragments were generated by annealing two complementary single-stranded oligonucleotides. They were then inserted into the *Age*I (#R3552S, NEB) site of the pTORA14 vector (Ohta *et al*, 2019) using the In-Fusion HD Cloning Kit. This yielded the pTORA14AAVS1, pTORA14CENP-B_C, pTORA14HA4, pTORA14HB7, and pTORA14HG1 plasmids, which were then used to induce DNA cleavage at the adeno-associated virus integration site 1 region of the *CENPB, HP1ALPHA, HP1BETA*, and *HP1GAMMA* genes, respectively. The DNA sequences targeted by the guide RNAs are listed in Table S2.

To construct the plasmid directing homologous recombination (HR) at the 3′ end of the *CENPB* gene, the DNA fragment was amplified via PCR on human genomic DNA by using Tks Gflex DNA polymerase (#R060A, Takara Bio) with the primers listed in Table S1. This yielded the 584-bp DNA fragment containing the 267-bp left homological arm (HRL) and 314-bp right homological arm (HRR) regions identical to the target locus. The amplified DNA fragment comprising the HRL and HRR regions was cloned into pCR-Blant (#K275020, Thermo Fisher Scientific). To construct the HR donor plasmids (pKANA1CENPB and pKANA2CENPB), the mAID cassettes containing the mAID-encoding region and either the hygromycin or blasticidin resistance genes were amplified using PCR on the template plasmid pMK287 or pMK288 (Natsume *et al*, 2016) and were inserted between the HRL and HRR regions using the In-Fusion HD Cloning Kit. The resultant plasmids were then used to generate the human cell line expressing the CENP-B:mAID fusion protein.

Cell culture

U2OS and HeLa cells were cultured in Dulbecco's modified Eagle's medium (DMEM; #044-29765, FUJIFILM Wako) supplemented with 10% (v/v) fetal bovine serum (Bovogen Biologicals), 100 U/mL of penicillin, and 100 μg/mL of streptomycin (#168-23191, Wako) at 37 °C in a humidified incubator maintained at 5% CO_2. To generate CENP-B^{OFF} cells, CENP-B conditional KO (cKO) cells were cultured with 0.2 μg/mL of Dox (#D3447, Sigma-Aldrich) for 24 h and subsequently with 0.5 mM of IAA (#094-07121, Wako) for 24 h prior to experimentation.

Cell lines

The HeLa-Int-03 human cell line consisting of approximately 15,000 repeats of the *tetO* sequence in chromosome 21 with and without CENP-B or HP1 KO was obtained as previously described (Ohzeki *et al*, 2012; Otake *et al*, 2020; Ruppert *et al*, 2018). The U2OS-*os*TIR1 cell line, which is the parental cell line of the CENP-B cKO cells, was generated by transfecting the U2OS cells with pTORA14AAVS1 and pMK243 (Natsume *et al*, 2016) using Lipofectamine LTX Reagent (#A12621, Thermo Fisher Scientific). The clone was selected by maintaining the culture with 1 μg/mL of puromycin (#10-2100, Focus Biomolecules). The CENP-B cKO cell line was generated by transfecting the U2OS-*os*TIR1 cell line with pTORA14CENP-B_C, pKANA1CENPB, and pKANA2CENPB. The clone was selected by maintaining the culture with 1 mg/mL of hygromycin B (#089-06151, Wako) and 5 μg/mL of blasticidin S (#ant-bl-05, InvivoGen).

Indirect immunofluorescence and microscopy

The U2OS and HeLa cells at the exponential growth phase were seeded onto coverslips at 30–40% confluence and allowed to grow overnight. To overexpress EGFP-ZNF518A and EGFP-ZNF518B, pDEST131NEGFP153 and pDEST131NEGFP127, respectively, were transfected into cells using Lipofectamine LTX for indirect immunofluorescence experiments. Twenty-four hours after the transfection, the cells were fixed with 4% (v/v) paraformaldehyde (#163-20145, Wako) in phosphate-buffered saline (PBS) for 10 min and permeabilized with 0.15% (v/v) Triton X-100 (#1610407, Bio-Rad Laboratories) in PBS for 2 min. The cells on the

coverslips were treated with 1% (v/v) bovine serum albumin (BSA; #A7284, Sigma-Aldrich) in PBS and subsequently with primary antibodies, including 1:200-diluted mouse anti-CENP-A (#ab13939, Abcam), 1:50,000-diluted mouse anti-CENP-B (5E6C1) (Okada *et al*, 2007), 1:200-diluted rabbit anti-CENP-B (#ab25734, Abcam), 1:600-diluted rabbit anti-CENP-C (#554) (Ohta *et al*, 2010b), 1:1,000-diluted mouse anti-HP1α (#MAB3584, Merck Millipore), 1:800-diluted rabbit anti-HP1β (#8676 D2F2, Cell Signaling Technology), 1:3,000-diluted mouse anti-HP1γ (#MAB3450 2MOD-1G6, Merck Millipore), or 1:1,000-diluted rabbit anti-histone H3K9me3 (#ab8898, Abcam). The cells were washed three times with PBS for 5 min and incubated with 1:600-diluted Alexa-conjugated secondary antibodies. The DNA was then stained with 0.1 μg/mL of DAPI (#H-1200, Vector Laboratories).

Confocal images were obtained using an Olympus FV1000 microscope, which is based on an IX81 confocal microscope system, with a UPlanSApo 60×/1.35 oil-immersion objective lens (Olympus) and FV10-SAW2.1 software (Olympus). Images were also obtained by the Nikon Confocal A1Rsi system, which is based on a Ti-E inverted microscope system, with a CFI Plan Apochromat VC 60×/1.40 oil-immersion objective lens (Nikon) and FNIS-Elements AR software (Nikon). The images were acquired at 0.5-μm intervals in the z-axis and Kalman-filtered to suppress background noise.

FMIT

The pDEST172JTY and pDEST155Halo plasmids encoding EYFP-TetR and Halo fusion proteins, respectively, were transfected into HeLa cells carrying the *tetO* array at 60% confluence using Lipofectamine 3000 (#L3000001, Thermo Fisher Scientific). Twenty-four hours after the transfection, the cells were further incubated with 1 nM of Halo Tag TMR Ligand (G825A, Promega) at 37 °C for 2 h. The labeled cells were washed with DMEM and incubated with the same medium at 37 °C for 30 min. The cells were subsequently fixed with 4% (v/v) paraformaldehyde in PBS for 10 min, and the DNA was stained with 0.1 μg/mL of DAPI. The EYFP and TMR signals were observed using the Olympus BX53 fluorescence microscope system with a UPlanSApo 60×/1.35 oil-immersion objective lens and cellSens standard software (Olympus). More than 100 cells were analyzed for each sample.

Quantification of microscopic data

Fluorescence quantitation and line plot analyses of the fluorescence signals were performed using ImageJ 1.50e for Mac (Schneider *et al*, 2012). To quantitate the fluorescent signals, z-stack images were captured at every 500 nm between the lower and upper edges of the nuclei and merged using the maximum intensity z-projection function in ImageJ. In the projected images, nuclei and centromeres were defined by DAPI and CENP-A signals, respectively. The nucleus- and centromere-associated GFP signals in the respective cells were then estimated, and a ratio between them was calculated to determine how GFP-fused proteins are enriched at centromeres. Statistical analyses were performed using R statistical software 3.5.1 (R Foundation for Statistical Computing, http://www.r-project.org).

For the line plot analyses, a specific slice showing the strongest signal of a centromeric protein (CENP-A or CENP-B) and GFP-ZNF518 was selected from the z-stack images. Using the RGB plot profile function in ImageJ, the signal intensity of the centromeric protein and GFP-ZNF518 was quantified for each pixel along the indicated lines.

Protein purification

The target proteins, His_6-GST-HP1 and HAT-MBP-ZNF518B$^{770-987}$, were purified from BL21 *E. coli* cells. To express the target proteins, *E. coli* cells carrying either pDEST173HGSTHP1 for His_6-GST-HP1 or pDEST174HATMBP127 for HAT-MBP-ZNF518B$^{770-987}$ were cultured at 30 °C for 2 h after adding IPTG (#096-05143, Wako) to L broth at a final concentration of 0.1 mM. A cell extract was prepared using a protein purification buffer containing 50 mM of Tris-HCl (pH 8.0; #201-06273, Wako), 500 mM of NaCl (#191-01665, Wako), 10 mM of β-mercaptoethanol (#131-14571, Wako), and 10% glycerol (#075-00611, Wako) for the His_6-GST-HP1 protein. For the HAT-MBP-ZNF518B$^{770-987}$ protein, a cell extract was prepared using the protein purification buffer with 1% Tween 20 (#H5152, Promega). The target proteins were then affinity-purified using Ni-NTA agarose (#143-09763, Wako).

MBP pull-down

All the procedures in the MBP pull-down (PD) experiments were performed with a PD buffer [25 mM of Tris-HCl (pH 8.0), 100 mM of NaCl, 1 mM of EDTA (#E5134, Sigma-

Aldrich), 1 μM of DTT (#GE17-1318-02, Sigma-Aldrich), 1% Tween 20, 10% glycerol, and 0.02% BSA]. First, 2 μg of HAT-MBP-ZNF518B$^{770-987}$ and 5 μg of His$_6$-GST-HP1 proteins, which had been purified as described above, were mixed and incubated with rotation at 4 °C for 4 h. Next, 50 μg of amylose magnetic beads (#E8035S, NEB) were added to the protein mixture and further incubated with rotation at 4 °C for 1 h. After washing the beads six times with 1 mL of the PD buffer, the sample was boiled with 1× SDS loading buffer at 95 °C for 5 min. The eluate was then subjected to immunoblotting.

Immunoblotting

Immunoblotting was carried out using primary antibodies, including 1:200-diluted mouse anti-MBP (#sc-271524, Santa Cruz Biotechnology) and mouse anti-GST (#sc-138, Santa Cruz Biotechnology), 1:1,000-diluted rabbit anti-HP1α (#2616, CST), mouse anti-HP1α (#MAB3584, Merck Millipore), 1:1,000-diluted rabbit anti-HP1β (#8676, CST), 1:1,000-diluted rabbit anti-HP1γ (#2619, CST), 1:1,000-diluted and mouse anti-HP1γ (#MAB3450, Merck Millipore), and 1:10,000-diluted mouse anti-GAPDH (#5A12,016-25523, Wako). The target proteins were then detected using 1:15,000-diluted IRDye 800CW donkey anti-rabbit IgG and 1:15,000-diluted anti-mouse IgG (#926-32213, #926-32210, Li-COR Biosciences) secondary antibodies.

Amino acid sequence analysis

The Basic Local Alignment Search Tool (BLAST) was used to identify similarities between query and amino acid sequences deposited in the DDBJ/GenBank/EMBL

databases (Altschul, 1990). A phylogenetic tree was constructed by the neighbor-joining method using MEGA X software (Kumar *et al*, 2018).

Acknowledgements

The authors thank Iyo Toramoto, Kana Yamazoe, and Fusako Kawasaki (Kochi University) for their technical assistance, Koichiro Otake (Kazusa DNA Research Institute) for providing preliminary data, Koichi Honke, Hideaki Kuge, Kaoru Miyahara, Arisa Miyagawa-Yamaguchi, and Tatsuyuki Yamashita (Kochi University) for their scientific advice, and William C Earnshaw (University of Edinburgh) for critically reading the manuscript. This work was supported by grants from JSPS KAKENHI (grant number 18K06061), Kato Memorial Bioscience Foundation, and Takeda Science Foundation to SO. This work was also supported by JST, CREST (grant number 18070874), partly by MEXT KAKENHI (grant number 20H00473), and the Kazusa DNA Research Institute Foundation to HM.

Author contributions

SO, JO and HM designed the study. SO, JO and NS performed the experiments. SO, JO and HM analyzed the data. SO, JO, KN and HM wrote the manuscript.

Disclosure and competing interests statement

The authors declare that they have no conflicts of interest.

Figure Legends

Figure 1. ZNF518B and its homolog ZNF518A localize to centromeres in a CENP-B-dependent manner.

(A, C, and E) Co-localization of GFP-ZNF518B (green) and the centromeric factors [red; CENP-A **(A),** CENP-B **(C),** or CENP-C **(E)**]. Areas marked by the open boxes in the left images are enlarged in the right panel. Scale bars indicate 5 μm.

(B, D, and F) Line plot analyses were carried out along the white lines in panels A, C, and E for the quantification of GFP-ZNF518B (green) and the three centromeric factors [red; CENP-A **(B)** CENP-B **(D)** and CENP-C **(F)**].

(G) Localization of GFP-ZNF518B (green) and CENP-A (red) in WT (upper) and CENP-B knockout cells (lower). The areas marked by the open boxes in the left panels are enlarged in the right panels.

(H) Quantification of the fluorescence intensities of GFP-ZNF518B signals at centromeres in WT, CENP-B knockout (KO) [see panel **(G)**], and CENP-B KO cells overexpressing CENP-B-$Flag_3$ [CENP-B KO + CENP-B-FL_3 OX; see panel **(I)**]. The y-axis shows the relative fluorescence intensities of GFP-ZNF518B signals associated with centromeres against total GFP signals in the nucleus. Open circles represent measurements from the individual cells shown in panels G and I. Red bars show medians. ***$p < 0.005$.

(I) Co-localization of GFP-ZNF518B (green), CENP-A (red), and CENP-B (blue) in CENP-B KO cells overexpressing CENP-B-$Flag_3$ (CENP-B KO + CENP-B-FL_3 OX). The area marked by the open box in the left panel is enlarged in the right panel.

(J) Co-localization of Halo-ZNF518A (red), GFP-ZNF518B (green), and CENP-A (blue). The area marked by the open box in the left panel is enlarged in the right panel.

Figure 2. Dissection of ZNF518B to identify its protein segments required for centromeric localization.

Localization of the ZFN518B derivatives at centromeres. The schematic representation of the respective ZNF518B derivatives is drawn approximately to scale. Yellow boxes indicate zinc-finger motifs. The two PxV(I)xL motifs (purple boxes) were substituted with KxSxS (light purple boxes), shown as KSS/N and KSS/C. KSS/NC indicates that both PxV(I)xLs motifs were substituted with KxSxS. GFP-fused ZNF518B signals (WT and 18 derivatives; green) were co-visualized with the CENP-A or CENP-B centromeric markers (left images). The two images (ZNF518B$^{KSS/NC}$ and ZNF518B$^{878-987}$) labeled with “A” show CENP-A foci, whereas the remaining images represent CENP-B signals. The areas marked by the open boxes in the left images are enlarged in the right panel. Numbers and colors (left) reflect % frequencies of cells with GFP-ZNF518B signals at pericentromeres. Scale bar indicates 5 μm.

Figure 3. The PxIxL motif in ZNF518B is required for its interaction with the chromo-shadow domain of HP1.

(A) Schematic diagram of the FMIT assay for investigating the interaction between ZNF518B and HP1. CENP-B KO cells were employed in this assay.

(B) Tethering YFP-ZNF518B (green) to the *tetO* repeats results in the accumulation of Halo-HP1β (top; red) but not Halo-HP1γ (bottom; red) at the locus.

(C) FMIT assay to examine the interaction between ZNF518B derivatives and HP1. Cells expressing TetR-EYFP-ZNF518B (WT or derivative) and Halo-HP1 were subjected to the FMIT assay. The ZNF518B segment predicted to interact with HP1 is indicated by shaded boxes. Numbers and colors reflect % frequencies of the co-localization of TetR-EYFP-ZNF518B with full-length HP1 (HP1α, HP1β, and HP1γ), and the chromo domain (CD) and chromo-shadow domain (CSD) of HP1β.

(D) Experimental design to examine whether ZNF518B is required to maintain HP1β localization at the *tetO* repeats. The TetR-EYFP-ZNF518 quickly dissociated from the *tetO* repeats in the presence of doxycycline (Dox). CENP-B KO cells were employed in this assay.

(E) Cells carrying TetR-EYFP-ZNF518 (WT or derivatives) and Halo-HP1β were subjected to the FMIT assay as explained in panel D.

(F) Pull-down (PD) experiments to examine the physical interactions between ZNF518B and HP1. Purified recombinant GST-HP1 (input) was incubated with MBP-ZNF518B$^{770\text{-}987}$, and MBP PD samples were subjected to immunoblotting using anti-GST. Signal intensities in the indicated samples were normalized by the intensities of the samples with MBP alone.

(G) A model depicting the central roles of ZNF518A and ZNF518B in pericentromeric heterochromatin formation via their interactions with CENP-B, HP1, and G9a. Molecules and arrows in color represent the reaction steps indicated in this figure.

Figure 4. Dissection of ZNF518B relative to its interaction with CENP-B.

(A) Schematic representation of the GFP-ZNF518B localization assay, where CENP-B was depleted by adding indole-3-acetic acid (IAA) at different times. Data are shown in panel B.

(B) Representative images of GFP-ZNF518B-transfected cells quantified in panels C and D**.** Localization of GFP-ZNF518B (green) relative to centromeres in CENP-B^{ON}, CENP-B^{OFF}, and CENP-B$^{4h\text{-}OFF}$ cells. CENP-A (red), CENP-B (blue), and DAPI staining are shown. The areas marked by the open boxes in the left images are enlarged in the right panel.

(C) Quantification of the fluorescence intensities of total CENP-B signals in CENP-B^{ON}, CENP-B^{OFF}, and CENP-B$^{4h\text{-}OFF}$ cells based on the images in panel B. ***$p < 0.005$, and red bars show medians. CENP-B signals in nuclei were measured.

(D) Quantification of the fluorescence intensities of GFP-ZNF518B signals at the pericentromeres in CENP-B^{ON}, CENP-B^{OFF}, and CENP-B$^{4h\text{-}OFF}$ cells based on the images shown in panel B. The y-axis shows the relative fluorescence intensities of GFP-ZNF518B signals associated with pericentromeres against total GFP signals in nuclei. Open circles represent measurements from the individual cells shown in panel B, and red bars show medians. **$p < 0.05$.

(E) Percentage of GFP-ZNF518B foci co-localized with centromeres (CENP-A foci) in CENP-B^{ON}, CENP-B^{OFF}, and CENP-B$^{4h\text{-}OFF}$ cells. The images in panel B were subjected to this analysis.

(F) Schematic diagram of the FMIT assay for investigating the interaction between ZNF518B and CENP-B. The CENP-B$^{133\text{-}599}$ derivative was used as it cannot bind to the alpha-satellite repeats at pericentromeres by itself.

(G) FMIT assay to quantify the co-localization between TetR-EYFP-ZNF518 and Halo-CENP-B$^{133-599}$. Numbers and colors reflect % frequencies of Halo-CENP-B$^{133-599}$ recruitment onto TetR-EYFP-ZNF518B foci. Red shaded boxes represent the ZNF518B segment predicted to be involved in the interaction with CENP-B$^{133-599}$.

(H) A model depicting the central roles of ZNF518A and ZNF518B in pericentromeric heterochromatin formation via their interactions with CENP-B, HP1, and G9a. Molecules and arrows in color represent the reaction steps indicated in the present figure.

Figure 5. Dissection of ZNF518A and ZNF518B relative to their requirement for the loading of G9a to centromeres.

(A) FMIT assay to quantify the co-localization between TetR-EYFP-ZNF518 (WT and 16 derivatives) and Halo-G9a. Green shaded boxes represent the ZNF518B segment potentially involved in its interaction with G9a.

(B) FMIT assay to quantify the co-localization between TetR-EYFP-ZNF518A (WT and seven derivatives) and Halo-G9a. Green shaded boxes represent the ZNF518A segment potentially involved in its interaction with G9a.

(C) FMIT assay to quantify the co-localization between Halo-G9a (WT and four derivatives) and either TetR-EYFP-ZNF518A or TetR-EYFP-ZNF518B.

(D) Co-visualization of Halo-G9a (red) and GFP-ZNF518B (WT and two derivatives) or GFP alone (green) in WT cells. The areas marked by the open boxes in the left images are enlarged in the right panel. Scale bar indicates 5 μm.

1 **(E)** Localization of Halo-G9a (red) and GFP-ZNF518B^{WT} (green) in CENP-B KO cells.

2 Scale bar indicates 5 μm.

3 **(F)** A model depicting the central roles of ZNF518A and ZNF518B in pericentromeric

4 heterochromatin formation via their interactions with CENP-B, HP1, and G9a (see

5 Discussion for details).

6

7

REFERENCES

Aagaard L, Laible G, Selenko P, Schmid M, Dorn R, Schotta G, Kuhfittig S, Wolf A, Lebersorger A, Singh PB, *et al* (1999) Functional mammalian homologues of the Drosophila PEV-modifier Su(var)3-9 encode centromere-associated proteins which complex with the heterochromatin component M31. *Embo J* 18: 1923–1938

Altschul S (1990) Basic Local Alignment Search Tool. *J Mol Biol* 215: 403–410

Amor DJ, Kalitsis P, Sumer H & Choo KHA (2004) Building the centromere: from foundation proteins to 3D organization. *Trends Cell Biol* 14: 359–368

Barra V & Fachinetti D (2018) The dark side of centromeres: types, causes and consequences of structural abnormalities implicating centromeric DNA. *Nat Commun* 9: 4340

Bergmann JH, Rodríguez MG, Martins NMC, Kimura H, Kelly DA, Masumoto H, Larionov V, Jansen LET & Earnshaw WC (2011) Epigenetic engineering shows H3K4me2 is required for HJURP targeting and CENP-A assembly on a synthetic human kinetochore. *The EMBO journal* 30: 328–340

Bian C, Chen Q & Yu X (2015) The zinc finger proteins ZNF644 and WIZ regulate the G9a/GLP complex for gene repression. *Elife* 4: e05606

Black BE & Cleveland DW (2011) Epigenetic Centromere Propagation and the Nature of CENP-A Nucleosomes. *Cell* 144: 471–479

Canzio D, Chang EY, Shankar S, Kuchenbecker KM, Simon MD, Madhani HD, Narlikar GJ & Al-Sady B (2011) Chromodomain-Mediated Oligomerization of HP1 Suggests a Nucleosome-Bridging Mechanism for Heterochromatin Assembly. *Mol Cell* 41: 67–81

Chaga G, Bochkariov DE, Jokhadze GG, Hopp J & Nelson P (1999) Natural poly-histidine affinity tag for purification of recombinant proteins on cobalt(II)-carboxymethylaspartate crosslinked agarose. *J Chromatogr A* 864: 247–256

1 Cheeseman IM & Desai A (2008) Molecular architecture of the kinetochore-microtubule
2 interface. *Nature reviews Molecular cell biology* 9: 33-46

3 Cleveland DW, Mao Y & Sullivan KF (2003) Centromeres and Kinetochores From
4 Epigenetics to Mitotic Checkpoint Signaling. *Cell* 112: 407-421

5 Du J & Patel DJ (2014) Structural biology-based insights into combinatorial readout and
6 crosstalk among epigenetic marks. *Biochimica Et Biophysica Acta Bba - Gene Regul*
7 *Mech* 1839: 719-727

8 Earnshaw W, Sullivan K, Machlin P, Cooke C, Kaiser D, Pollard T, Rothfield N & Cleveland
9 D (1987) Molecular cloning of cDNA for CENP-B, the major human centromere
10 autoantigen. *J Cell Biology* 104: 817-829

11 Fritsch L, Robin P, Mathieu JRR, Souidi M, Hinaux H, Rougeulle C, Harel-Bellan A,
12 Ameyar-Zazoua M & Ait-Si-Ali S (2010) A Subset of the Histone H3 Lysine 9
13 Methyltransferases Suv39h1, G9a, GLP, and SETDB1 Participate in a Multimeric
14 Complex. *Mol Cell* 37: 46-56

15 Grewal SIS & Jia S (2007) Heterochromatin revisited. *Nat Rev Genet* 8: 35-46

16 Hyun K, Jeon J, Park K & Kim J (2017) Writing, erasing and reading histone lysine
17 methylations. *Exp Mol Medicine* 49: e324-e324

18 Itoh M, Yasunishi A, Imamura K, Kanamori-Katayama M, Suzuki H, Suzuki M, Carninci P,
19 Kawai J & Hayashizaki Y (2006) Constructing ORFeome resources with removable
20 termination codons. *Biotechniques* 41: 44-50

21 Kimura K, Wakamatsu A, Suzuki Y, Ota T, Nishikawa T, Yamashita R, Yamamoto J, Sekine
22 M, Tsuritani K, Wakaguri H, *et al* (2006) Diversification of transcriptional modulation:
23 Large-scale identification and characterization of putative alternative promoters of
24 human genes. *Genome Res* 16: 55-65

25 Kumar S, Stecher G, Li M, Knyaz C & Tamura K (2018) MEGA X: Molecular Evolutionary
26 Genetics Analysis across Computing Platforms. *Mol Biol Evol* 35: 1547-1549

27 Maier VK, Feeney CM, Taylor JE, Creech AL, Qiao JW, Szanto A, Das PP, Chevrier N,
28 Cifuentes-Rojas C, Orkin SH, *et al* (2015) Functional Proteomic Analysis of Repressive

Histone Methyltransferase Complexes Reveals ZNF518B as a G9A Regulator. *Molecular & cellular proteomics : MCP* 14: 1435-1446

Martin C & Zhang Y (2005) The diverse functions of histone lysine methylation. *Nat Rev Mol Cell Bio* 6: 838-849

Martins NMC, Bergmann JH, Shono N, Kimura H, Larionov V, Masumoto H & Earnshaw WC (2016) Epigenetic engineering shows that a human centromere resists silencing mediated by H3K27me3/K9me3. *Molecular biology of the cell* 27: 177-196

Masumoto H, Nakano M & Ohzeki J (2004) The role of CENP-B and α-satellite DNA: de novo assembly and epigenetic maintenance of human centromeres. *Chromosome Res* 12: 543-556

McKinley KL & Cheeseman IM (2016) The molecular basis for centromere identity and function. *Nat Rev Mol Cell Bio* 17: 16-29

Molina O, Abad MA, Solé F & Menéndez P (2020) Aneuploidy in Cancer: Lessons from Acute Lymphoblastic Leukemia. *Trends Cancer* 7: 37-47

Molina O, Vargiu G, Abad MA, Zhiteneva A, Jeyaprakash AA, Masumoto H, Kouprina N, Larionov V & Earnshaw WC (2016) Epigenetic engineering reveals a balance between histone modifications and transcription in kinetochore maintenance. *Nature communications* 7: 13334

Muramatsu D, Kimura H, Kotoshiba K, Tachibana M & Shinkai Y (2016) Pericentric H3K9me3 formation by HP1 interaction-defective histone methyltransferase Suv39h1. *Cell Struct Funct* 41: 145-152

Nagase T, Yamakawa H, Tadokoro S, Nakajima D, Inoue S, Yamaguchi K, Itokawa Y, Kikuno RF, Koga H & Ohara O (2008) Exploration of Human ORFeome: High-Throughput Preparation of ORF Clones and Efficient Characterization of Their Protein Products. *Dna Res* 15: 137-149

Natsume T, Kiyomitsu T, Saga Y & Kanemaki MT (2016) Rapid Protein Depletion in Human Cells by Auxin-Inducible Degron Tagging with Short Homology Donors. *Cell reports* 15: 210-218

Ohta S, Bukowski-Wills J-C, Sanchez-Pulido L, Alves F de L, Wood L, Chen ZA, Platani M, Fischer L, Hudson DF, Ponting CP, *et al* (2010a) The Protein Composition of Mitotic Chromosomes Determined Using Multiclassifier Combinatorial Proteomics. *Cell* 142: 810-821

Ohta S, Bukowski-Wills J-C, Wood L, Alves F de L, Chen Z, Rappsilber J & Earnshaw WC (2010b) Proteomics of isolated mitotic chromosomes identifies the kinetochore protein Ska3/Rama1. *Cold Spring Harbor symposia on quantitative biology* 75: 433-438

Ohta S, Hamada M, Sato N & Toramoto I (2015) Polyglutamylated Tubulin Binding Protein C1orf96/CSAP Is Involved in Microtubule Stabilization in Mitotic Spindles. *PloS one* 10: e0142798

Ohta S, Montaňo-Gutierrez LF, Alves F de L, Ogawa H, Toramoto I, Sato N, Morrison CG, Takeda S, Hudson DF, Rappsilber J, *et al* (2016) Proteomics analysis with a nano Random Forest approach reveals novel functional interactions regulated by SMC complexes on mitotic chromosomes. *Molecular & cellular proteomics : MCP* 15: 2802-2818

Ohta S, Taniguchi T, Sato N, Hamada M, Taniguchi H & Rappsilber J (2019) Quantitative Proteomics of the Mitotic Chromosome Scaffold Reveals the Association of BAZ1B with Chromosomal Axes*[S]. *Mol Cell Proteomics* 18: 169-181

Ohzeki J, Bergmann JH, Kouprina N, Noskov VN, Nakano M, Kimura H, Earnshaw WC, Larionov V & Masumoto H (2012) Breaking the HAC Barrier: histone H3K9 acetyl/methyl balance regulates CENP-A assembly. *The EMBO journal* 31: 2391-2402

Ohzeki J, Nakano M, Okada T & Masumoto H (2002) CENP-B box is required for de novo centromere chromatin assembly on human alphoid DNA. *The Journal of cell biology* 159: 765-775

Ohzeki J, Shono N, Otake K, Martins NMC, Kugou K, Kimura H, Nagase T, Larionov V, Earnshaw WC & Masumoto H (2016) KAT7/HBO1/MYST2 Regulates CENP-A Chromatin Assembly by Antagonizing Suv39h1-Mediated Centromere Inactivation. *Developmental cell* 37: 413-427

1 Okada T, Ohzeki J, Nakano M, Yoda K, Brinkley WR, Larionov V & Masumoto H (2007)
2 CENP-B controls centromere formation depending on the chromatin context. *Cell* 131:
3 1287-1300

4 Okamoto Y, Nakano M, Ohzeki J, Larionov V & Masumoto H (2007) A minimal CENP-A
5 core is required for nucleation and maintenance of a functional human centromere.
6 *Embo J* 26: 1279-1291

7 Ota T, Suzuki Y, Nishikawa T, Otsuki T, Sugiyama T, Irie R, Wakamatsu A, Hayashi K, Sato
8 H, Nagai K, *et al* (2004) Complete sequencing and characterization of 21,243 full-length
9 human cDNAs. *Nature genetics* 36: 40-45

10 Otake K, Ohzeki J, Shono N, Kugou K, Okazaki K, Nagase T, Yamakawa H, Kouprina N,
11 Larionov V, Kimura H, *et al* (2020) CENP-B creates alternative epigenetic chromatin
12 states permissive for CENP-A or heterochromatin assembly. *J Cell Sci* 133: jcs243303

13 Otsuki T, Ota T, Nishikawa T, Hayashi K, Suzuki Y, Yamamoto J, Wakamatsu A, Kimura K,
14 Sakamoto K, Hatano N, *et al* (2005) Signal Sequence and Keyword Trap in silico for
15 Selection of Full-Length Human cDNAs Encoding Secretion or Membrane Proteins
16 from Oligo-Capped cDNA Libraries. *Dna Res* 12: 117-126

17 Peters AHFM, O'Carroll D, Scherthan H, Mechtler K, Sauer S, Schöfer C,
18 Weipoltshammer K, Pagani M, Lachner M, Kohlmaier A, *et al* (2001) Loss of the Suv39h
19 Histone Methyltransferases Impairs Mammalian Heterochromatin and Genome Stability.
20 *Cell* 107: 323-337

21 Rea S, Eisenhaber F, O'Carroll D, Strahl BD, Sun Z-W, Schmid M, Opravil S, Mechtler K,
22 Ponting CP, Allis CD, *et al* (2000) Regulation of chromatin structure by site-specific
23 histone H3 methyltransferases. *Nature* 406: 593-599

24 Ruppert JG, Samejima K, Platani M, Molina O, Kimura H, Jeyaprakash AA, Ohta S &
25 Earnshaw WC (2018) HP1α targets the chromosomal passenger complex for
26 activation at heterochromatin before mitotic entry. *Embo J* 37

27 Schneider CA, Rasband WS & Eliceiri KW (2012) NIH Image to ImageJ: 25 years of image
28 analysis. *Nat Methods* 9: 671-675

1 Schueler MG & Sullivan BA (2006) Structural and Functional Dynamics of Human
2 Centromeric Chromatin. *Annu Rev Genom Hum G* 7: 301–313

3 Shirai A, Kawaguchi T, Shimojo H, Muramatsu D, Ishida-Yonetani M, Nishimura Y, Kimura
4 H, Nakayama J-I & Shinkai Y (2017) Impact of nucleic acid and methylated H3K9
5 binding activities of Suv39h1 on its heterochromatin assembly. *eLife* 6

6 Shono N, Ohzeki J, Otake K, Martins NMC, Nagase T, Kimura H, Larionov V, Earnshaw WC
7 & Masumoto H (2015) CENP-C and CENP-I are key connecting factors for
8 kinetochore and CENP-A assembly. *J Cell Sci* 128: 4572–4587

9 Simon JM, Parker JS, Liu F, Rothbart SB, Ait-Si-Ali S, Strahl BD, Jin J, Davis IJ, Mosley
10 AL & Pattenden SG (2015) A Role for Widely Interspaced Zinc Finger (WIZ) in
11 Retention of the G9a Methyltransferase on Chromatin*. *J Biol Chem* 290: 26088–
12 26102

13 Sullivan BA & Karpen GH (2004) Centromeric chromatin exhibits a histone modification
14 pattern that is distinct from both euchromatin and heterochromatin. *Nat Struct Mol*
15 *Biol* 11: 1076–1083

16 Tachibana M, Sugimoto K, Fukushima T & Shinkai Y (2001) SET Domain-containing
17 Protein, G9a, Is a Novel Lysine-preferring Mammalian Histone Methyltransferase with
18 Hyperactivity and Specific Selectivity to Lysines 9 and 27 of Histone H3*. *J Biol Chem*
19 276: 25309–25317

20 Thiru A, Nietlispach D, Mott HR, Okuwaki M, Lyon D, Nielsen PR, Hirshberg M, Verreault
21 A, Murzina NV & Laue ED (2004) Structural basis of HP1/PXVXL motif peptide
22 interactions and HP1 localisation to heterochromatin. *The EMBO journal* 23: 489–499

23 Ueda J, Tachibana M, Ikura T & Shinkai Y (2006) Zinc Finger Protein Wiz Links G9a/GLP
24 Histone Methyltransferases to the Co-repressor Molecule CtBP*. *J Biol Chem* 281:
25 20120–20128

26 Waye JS & Willard HF (1987) Nucleotide sequence heterogeneity of alpha satellite
27 repetitive DNA: a survey of alphoid sequences from different human chromosomes.
28 *Nucleic Acids Res* 15: 7549–7569

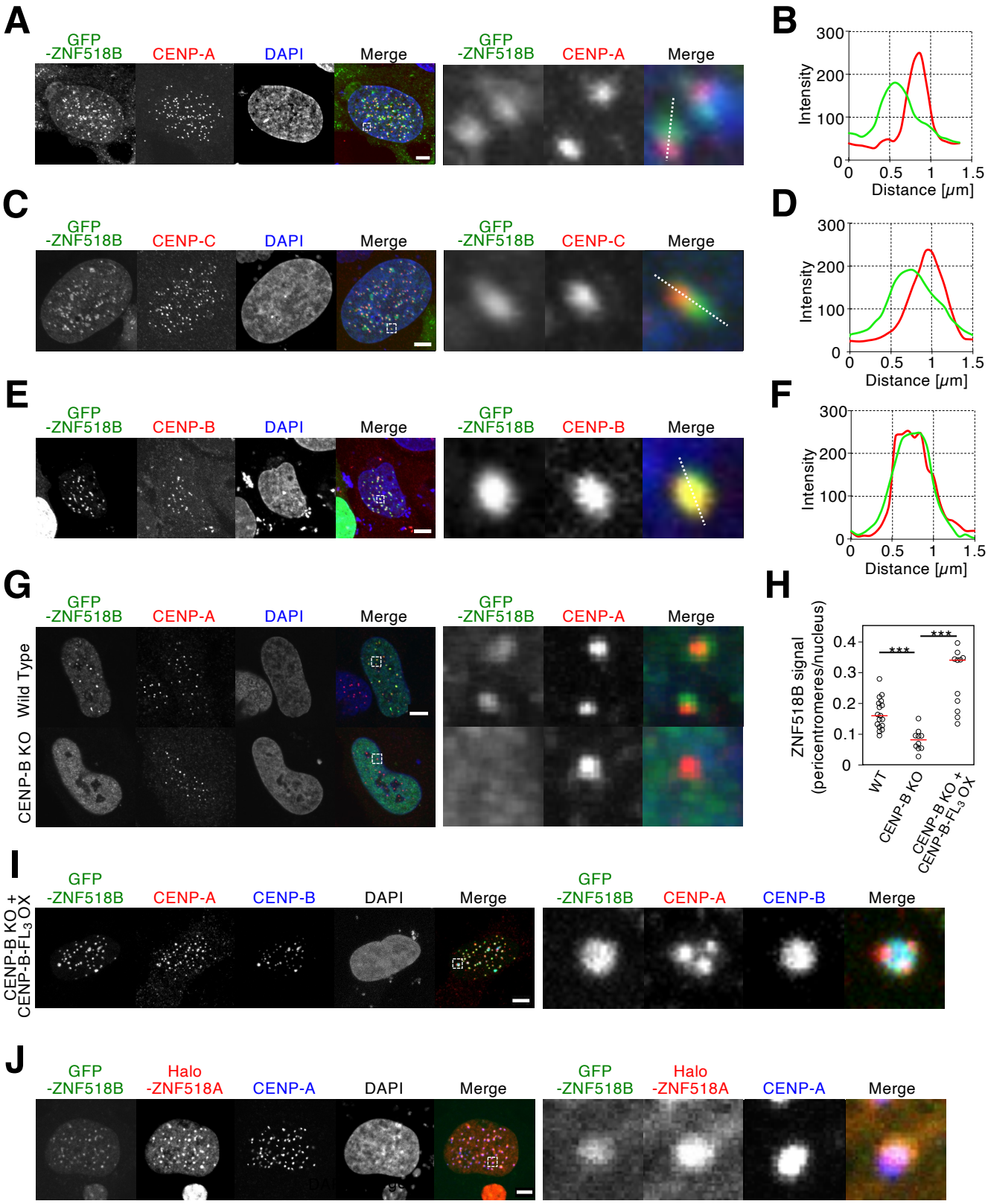
A
GFP -ZNF518B
CENP-A
DAPI
Merge
B
Intensity
Distance [μm]
C
CENP-C
D
E
CENP-B
F
G
Wild Type
CENP-B KO
H
ZNF518B signal (pericentromeres/nucleus)
WT
CENP-B KO
CENP-B KO + CENP-B-FL3 OX
I
CENP-B KO + CENP-B-FL3 OX
J
Halo -ZNF518A

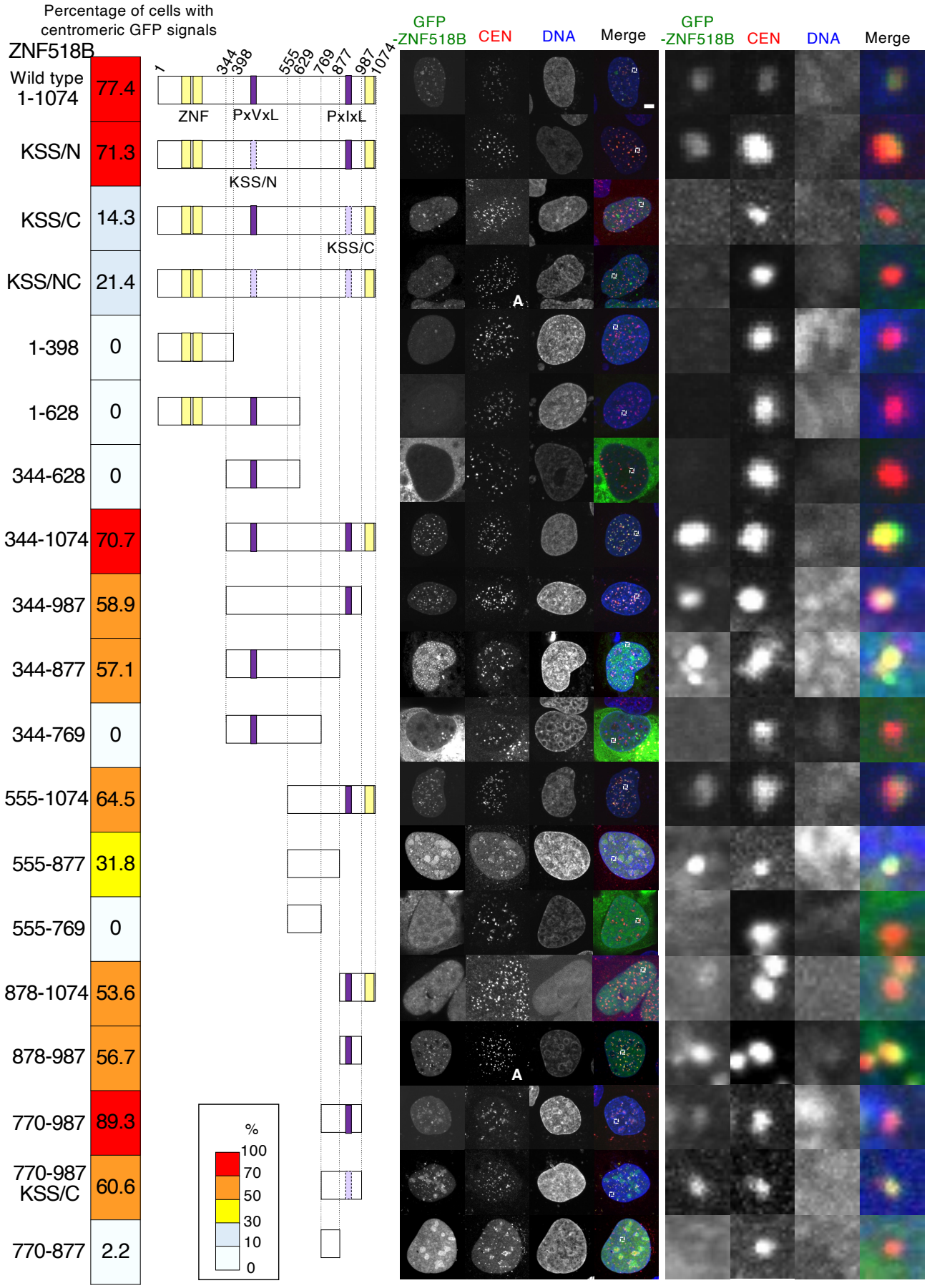
Percentage of cells with centromeric GFP signals
ZNF518B
Wild type 1-1074 77.4
KSS/N 71.3
KSS/C 14.3
KSS/NC 21.4
1-398 0
1-628 0
344-628 0
344-1074 70.7
344-987 58.9
344-877 57.1
344-769 0
555-1074 64.5
555-877 31.8
555-769 0
878-1074 53.6
878-987 56.7
770-987 89.3
770-987 KSS/C 60.6
770-877 2.2
1
344
398
555
629
769
877
987
1074
ZNF
PxVxL
PxIxL
KSS/N
KSS/C
%
100
70
50
30
10
0
GFP -ZNF518B
CEN
DNA
Merge
A

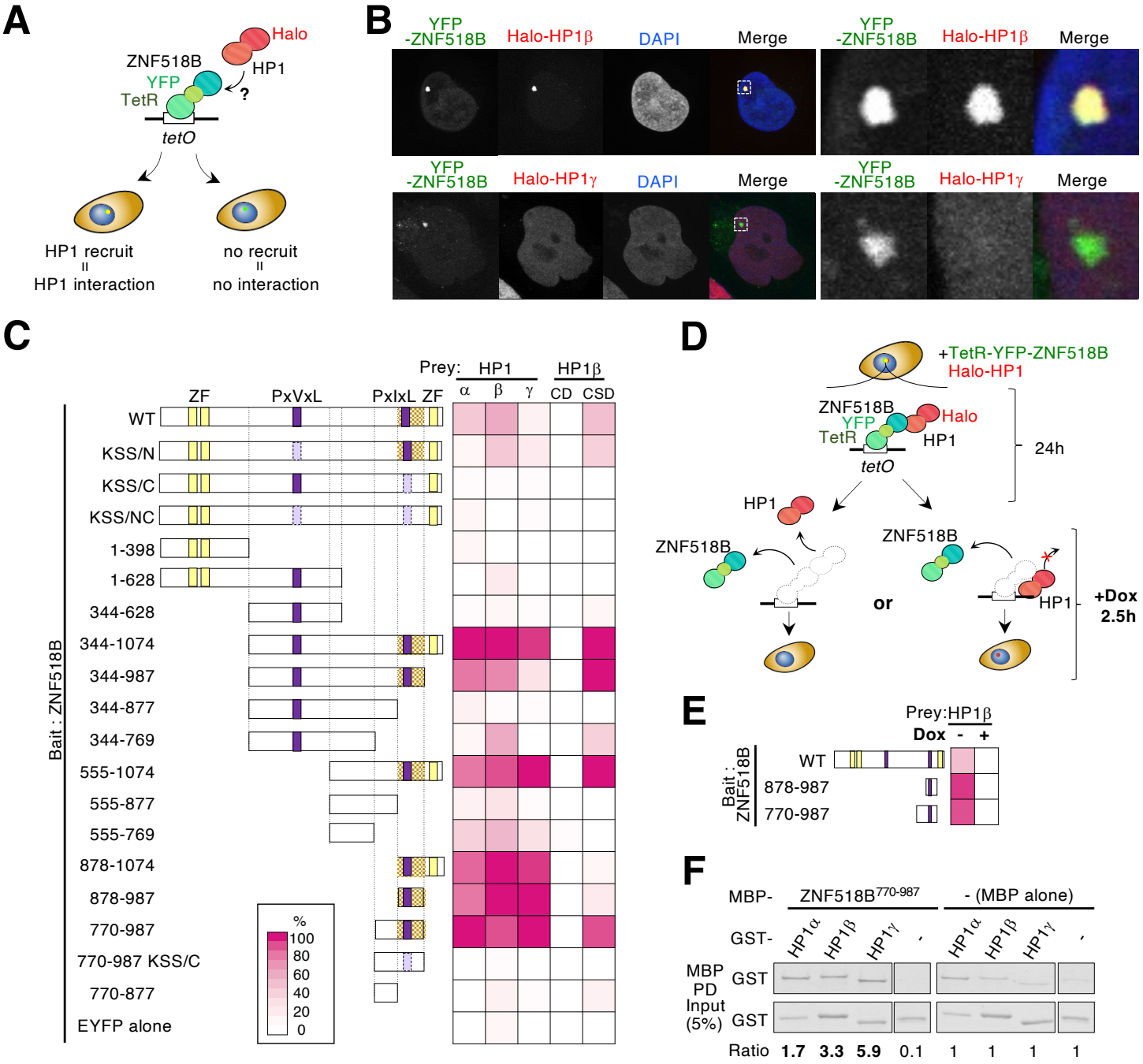
A
Halo
ZNF518B
HP1
YFP
TetR
?
tetO
HP1 recruit
=
HP1 interaction
no recruit
=
no interaction
B
YFP -ZNF518B
Halo-HP1β
DAPI
Merge
YFP -ZNF518B
Halo-HP1β
Merge
YFP -ZNF518B
Halo-HP1γ
DAPI
Merge
YFP -ZNF518B
Halo-HP1γ
Merge
C
Prey: HP1 HP1β
α β γ CD CSD
ZF PxVxL PxIxL ZF
Bait : ZNF518B
WT
KSS/N
KSS/C
KSS/NC
1-398
1-628
344-628
344-1074
344-987
344-877
344-769
555-1074
555-877
555-769
878-1074
878-987
770-987
770-987 KSS/C
770-877
EYFP alone
%
100
80
60
40
20
0
D
+TetR-YFP-ZNF518B
Halo-HP1
ZNF518B
YFP
TetR
Halo
HP1
tetO
24h
HP1
ZNF518B
ZNF518B
or
HP1
+Dox
2.5h
E
Prey:HP1β
Dox - +
Bait : ZNF518B
WT
878-987
770-987
F
MBP- ZNF518B770-987 - (MBP alone)
GST- HP1α HP1β HP1γ - HP1α HP1β HP1γ -
MBP PD GST
Input (5%) GST
Ratio 1.7 3.3 5.9 0.1 1 1 1 1
G
N
ZNF
PVL
ZNF518
CENP-B
C
HTH
B-box
ZNF518 loading
to pericentromeres
ZNF518
HP1β
CSD
CD
Stable complex
formation
G9a
G9a loading
to pericentromeres
G9a-mediated H3K9me

Ohta *et al.*, Fig. 4

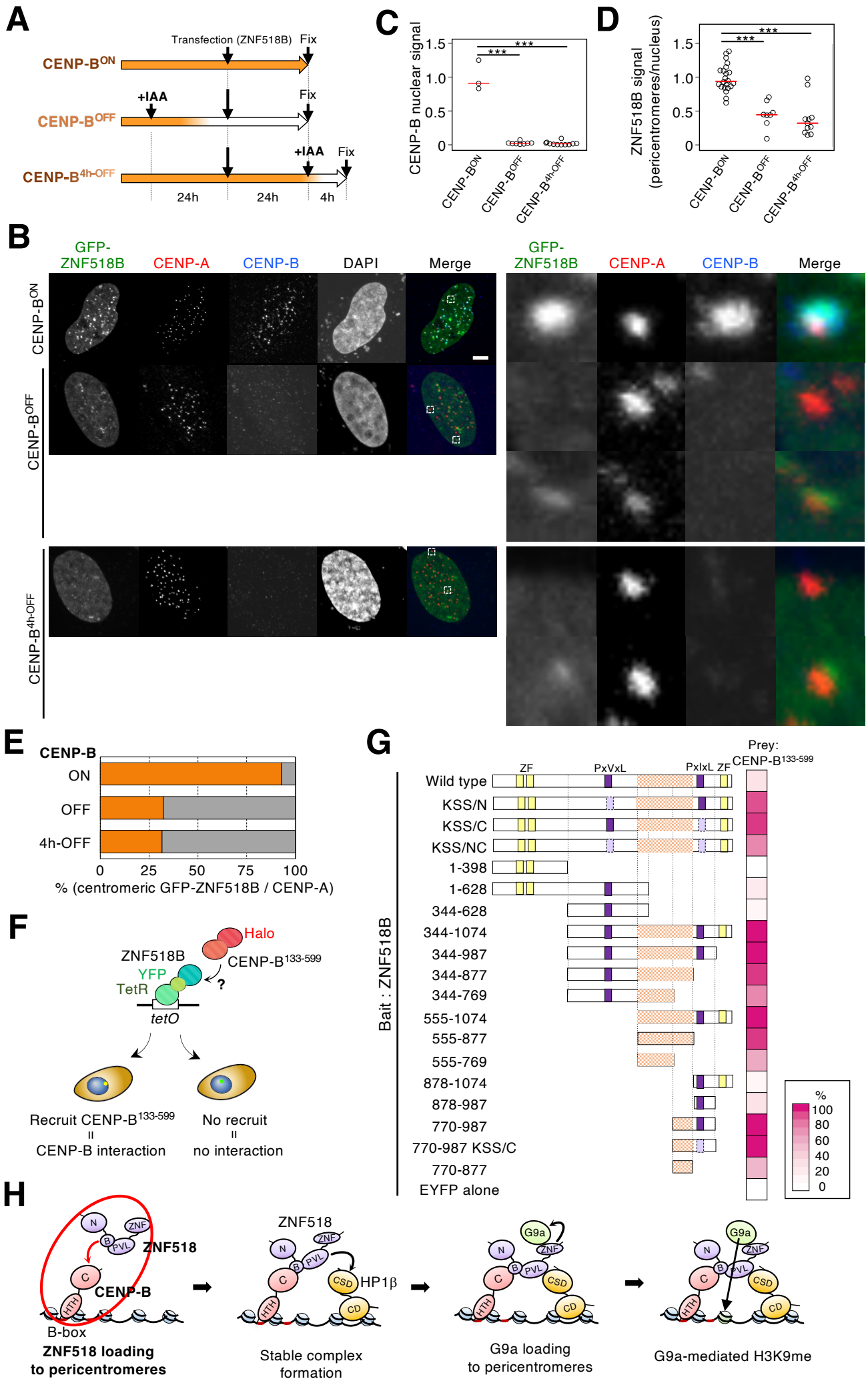

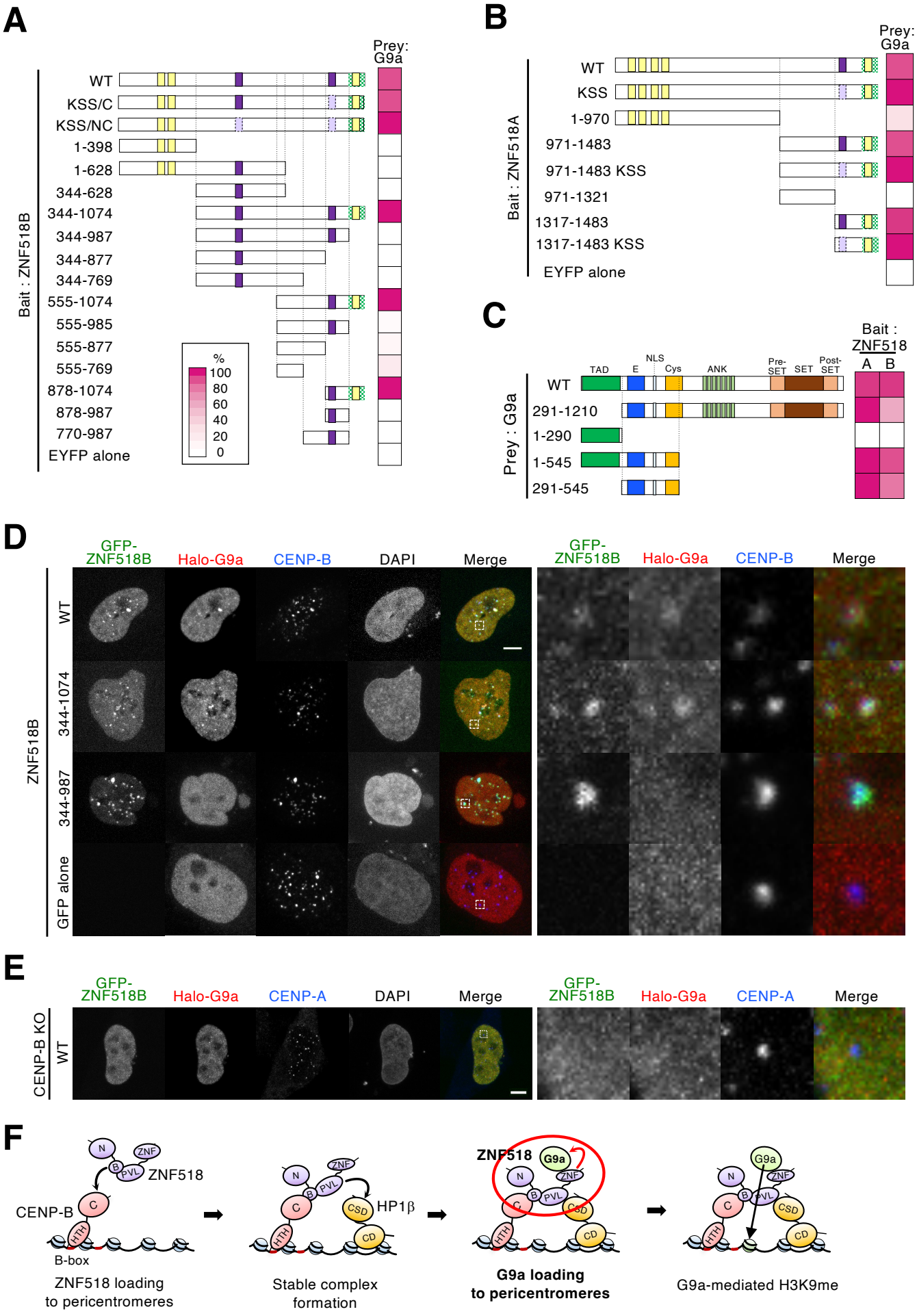
A
Prey: G9a
Bait : ZNF518B
WT
KSS/C
KSS/NC
1-398
1-628
344-628
344-1074
344-987
344-877
344-769
555-1074
555-985
555-877
555-769
878-1074
878-987
770-987
EYFP alone
%
100
80
60
40
20
0
B
Prey: G9a
Bait : ZNF518A
WT
KSS
1-970
971-1483
971-1483 KSS
971-1321
1317-1483
1317-1483 KSS
EYFP alone
C
Bait : ZNF518
A B
TAD
E
NLS
Cys
ANK
Pre-SET
SET
Post-SET
Prey : G9a
WT
291-1210
1-290
1-545
291-545
D
GFP-ZNF518B
Halo-G9a
CENP-B
DAPI
Merge
ZNF518B
WT
344-1074
344-987
GFP alone
E
GFP-ZNF518B
Halo-G9a
CENP-A
DAPI
Merge
CENP-B KO
WT
F
N
ZNF
B
PVL
ZNF518
CENP-B
C
HTH
B-box
ZNF518 loading to pericentromeres
HP1β
CSD
CD
Stable complex formation
G9a
G9a loading to pericentromeres
G9a-mediated H3K9me